Absence of complex I is associated with diminished respiratory chain function in European mistletoe

Subtitle: Multicellular life without respiratory complex I

Andrew E. Maclean[1,2], Alexander P. Hertle[3], Joanna Ligas[3], Ralph Bock[3], Janneke Balk[1,2], and Etienne H. Meyer[3]*

[1]Department of Biological Chemistry, John Innes Centre, Colney Lane, Norwich NR4 7UH, UK
[2] School of Biological Sciences, University of East Anglia, Norwich Research Park, Norwich NR4 7TJ, UK
[3] Max-Planck-Institute of Molecular Plant Physiology, Am Mühlenberg 1, D-14471 Potsdam-Golm, Germany

*Author for correspondence, emeyer@mpimp-golm.mpg.de

Lead Contact: Etienne H. Meyer

Summary

Parasitism is a life history strategy found across all domains of life whereby nutrition is obtained from a host. It is often associated with reductive evolution of the genome, including loss of genes from the organellar genomes [1,2]. In some unicellular parasites, the mitochondrial genome (mitogenome) has been lost entirely, with far-reaching consequences for the physiology of the organism [3,4]. Recently, mitogenome sequences of several species of the hemiparasitic plant mistletoe (*Viscum* sp.) have been reported [5,6], revealing a striking loss of genes not seen in any other multicellular eukaryotes. In particular, the *nad* genes encoding subunits of respiratory complex I are all absent and other protein-coding genes are also lost or highly diverged in sequence, raising the question what remains of the respiratory complexes and mitochondrial functions. Here we show that oxidative phosphorylation (OXPHOS) in European mistletoe, *Viscum album,* is highly diminished. Complex I activity and protein subunits of complex I could not be detected. The levels of complex IV and ATP synthase were at least 5-fold lower than in the non-parasitic model plant *Arabidopsis thaliana*, whereas alternative dehydrogenases and oxidases were higher in abundance. Carbon flux analysis indicates that cytosolic reactions including glycolysis are greater contributors to ATP synthesis than the mitochondrial TCA cycle. Our results describe the extreme adjustments in mitochondrial functions of the first reported multicellular eukaryote without complex I.

Results and Discussion

The size of plant mitogenomes varies enormously in size, from 101 kb in the moss *Buxbaumia aphyll* [7] to 11.3 Mb in *Silene conica* [8], but gene content is less variable, typically comprising ~20 - 41 protein coding genes for subunits of complexes I - V, the mitochondrial ribosome, cytochrome *c* maturation, 3 rRNAs and a variable number of tRNAs [9]. The Malaysian mistletoe *Viscum scurruloideum* has an unusually small mitogenome of 66 kb, making it the smallest land plant mitogenome sequenced to date [5]. Out of 24 core genes found in virtually all angiosperm mitogenomes, *V. scurruloideum* has lost all 9 *nad* genes coding for subunits of complex I as well as the maturase gene *matR*, the cytochrome *c* biosynthesis gene *ccmB* and genes for some ribosomal proteins. The *V. scurruloideum* mitogenome has retained genes for complex II (*sdh4*), III (*cob*), IV (*cox1*, *cox2* and *cox3*) and V (*atp1*, *atp4*, *atp6*, *atp8* and *atp9*), genes for 5 ribosomal proteins, the genes for two cytochrome c maturation factors (*ccmC* and *ccmF*), and the protein transporter *mttB*. Extensive mitochondrial gene loss has also been found in other species of mistletoe [6]. Although the mitogenome of European mistletoe, *Viscum album,* is substantially bigger (565 kb), a similar pattern of gene loss was observed, including the absence of all 9 *nad* genes, but not *matR* [10]. Mitochondrial genes can be transferred to the nucleus, for example *nad7* in *Marchantia polymorpha* [11], but it is highly unlikely that this would have happened for all 9 *nad* genes.

The loss of complex I has occurred several times during evolution, but so far, this has only been found in unicellular eukaryotes. In several anaerobes, OXPHOS is lost completely, but in four lineages of respiring eukaryotes, complex I is lost, including the yeast *Saccharomyces* [12-14]. Here we provide evidence for the lack of complex I in *Viscum album and* uncover dramatic changes in mitochondrial functions of this multicellular plant species.

To investigate the ultrastructure of *Viscum* mitochondria, leaf mesophyll cells were studied by electron microscopy. Small oval organelles of 0.6 - 1.1 µm in length were seen, surrounded by a double membrane (Figure 1A). The presence of internal membrane structures reminiscent of cristae indicated that these are mitochondria. In contrast to mitochondria in other plants species, the number of cristae is very low. In addition, there was poor staining in the matrix, and no ribosomes were seen, suggesting a low rate of translation of mitochondrially encoded genes.

To purify mitochondria for proteomic and biochemical studies, we used protocols developed for *Arabidopsis* based on differential centrifugation steps and density gradient centrifugation

[15,16]. Two different *Viscum album* populations were sampled, one in the UK and one in Germany, which gave similar results for all our subsequent analyses. Details on locations and host trees for each experiment can be found in Table S1. Terminal leaf buds were used as source material (Figure 1B), as initial purification attempts with leaves had failed because the extracts were very viscous and had high levels of chloroplast contamination. The mitochondria sedimented towards the bottom of the gradient, whereas thylakoids were retained at the top of the gradient (Figure 1C). The mitochondrial fraction was collected and washed, yielding 0.25 – 1 mg mitochondria from 50 g starting material. To verify the enrichment in mitochondrial protein, western blot analysis with antibodies against mitochondrial marker proteins was performed (Figure 1D).

To test for the presence of respiratory complexes in *Viscum*, mitochondrial membranes were solubilized with dodecylmaltoside and separated by Blue-Native Polyacrylamide Gel Electrophoresis (BN-PAGE). Gels were stained with Coomassie Blue to visualise mitochondrial protein complexes, and compared to mitochondria isolated from an *Arabidopsis thaliana* cell culture (Figure 2A). In the *Arabidopsis* sample, the abundant protein complexes I, V and III (from top to bottom) are clearly resolved. The *Viscum* sample also contained numerous bands at high molecular weight, but these were less abundant and did not match the pattern in Arabidopsis.

To identify the respiratory complexes in *Viscum*, in-gel enzyme activity stains were performed on *Arabidopsis* and *Viscum* mitochondria separated by BN-PAGE. NADH:NBT staining to visualise NADH dehydrogenase activities, including complex I, revealed an activity at approximately 146 kDa in both samples, which was previously attributed to lipoamide dehydrogenase (LPD2), a component of mitochondrial alpha-ketoacid dehydrogenase complexes [17] (Figure 2B). Detection of this activity served as additional confirmation that both samples were similarly enriched in mitochondria. In the *Arabidopsis* sample, a clear activity band can be seen at ~1 MDa which represents respiratory complex I. This band is completely absent from *Viscum* mitochondria (Figure 2B). Additional in-gel enzyme activity stains confirmed the presence of complex II in *Viscum* at ~142 kDa (Figure 2C). Complex III could also be detected, albeit less prominently than in Arabidopsis, through visualisation of the peroxidase activity of heme cofactors (Figure 2D). Complex IV was detected using reduced cytochrome *c* and diaminobenzidine, but a much lower activity was found in *Viscum* compared to *Arabidopsis* (Figure 2E). Taken together, these data show the presence of complex II, decreased amounts of complexes III and IV, and they are consistent with the proposed absence of respiratory complex I from *Viscum*.

To gain further insights into biochemical functions of mitochondria in *Viscum*, we performed proteomic analyses of whole mitochondria by LC-MS/MS. Because the nuclear genome of *Viscum album*, estimated to be 201 Gb in size [18], has not been sequenced to date, we used the *Arabidopsis* proteome as reference for protein identification. A simulation was carried out to show that sample complexity was similar between *Arabidopsis* and *Viscum* and that 30 to 40 % of the *Viscum* mitochondrial proteins could be identified using Arabidopsis sequences (Data S1). We identified between 384 and 492 proteins per replicate (n=3) and built a list of 292 proteins that were confidently identified in at least two replicates (Data S1). Of these 292 proteins, 282 have a predicted mitochondrial localization, and 193 have been experimentally confirmed in Arabidopsis (http://suba.live/). Moreover, we found that the *Arabidopsis* and *Viscum* mitochondrial samples contained similar, but low (3%) levels of likely non-mitochondrial proteins (Data S1). We then determined which biological processes are significantly enriched in our purified mitochondria using the gene ontology (GO) enrichment tool (geneontology.org). In *Arabidopsis*, there is, as expected, an enrichment of proteins of the electron transfer chain and the mitochondrial ATP synthase. By contrast, fewer components of the respiratory chain are detected in *Viscum*, leading to a non-significant enrichment (Figure 3A, Table S2). Because we used the *Arabidopsis* proteome as reference to identify mitochondrial protein in *Viscum*, this GO enrichment analysis suggests that the respiratory chain is either highly divergent between *Arabidopsis* and *Viscum* or depleted in *Viscum*. Other mitochondrial functions (e.g. mitochondria organisation, TCA cycle, vitamin biosynthesis) are similarly enriched in both samples, indicating that they are conserved and demonstrating that comparable numbers of proteins involved in these pathways are detectable in both species (Figure 3A, Table S2).

We also performed complexome profiling to identify and quantify proteins that are assembled in higher mass complexes. Mitochondria extracted from *Arabidopsis* and *Viscum* were solubilized, and protein complexes were separated by BN-PAGE. Each lane was divided into 18 gel slices of equal size which were then analysed by mass spectrometry (Figure S1A). Using label-free quantification, the abundance profiles of selected proteins were extracted. For the respiratory complexes II to V, a number of subunits were detected in *Viscum*, albeit at decreased levels compared to Arabidopsis (Figure S1B). The profiles of two proteins involved in housekeeping functions, HSP60 and ANT1, suggest that an equal amount of mitochondria was loaded in each lane (Figure S1C).

To obtain a more quantitative overview of differences in mitochondrial functions between *Viscum* and *Arabidopsis*, we extracted abundance data of individual peptides for 137 proteins from both proteomic approaches. The proteins were divided into functional groups, and the average abundance of the proteins in each group served as an indicator of the

relative prominence of a functional pathway in *Viscum* relative to *Arabidopsis*. (Figure 3B, Data S2). We found that proteins involved in primary metabolism (TCA cycle, respiratory chain, photorespiration, amino acid metabolism) and in mitochondrial translation are less abundant in *Viscum* than in *Arabidopsis*. However, other mitochondrial functions (e.g., cofactor biosynthesis, transport, genome maintenance) are not decreased in *Viscum*. For the respiratory chain, subunits of complexes II, III, IV and V, but none of complex I, were detected. Moreover, the abundance of complexes II-V was decreased compared to *Arabidopsis* (to 14-44% of the Arabidopsis levels). This result is in good agreement with the in-gel activity staining of respiratory complexes (Figure 2), although our complexome analysis suggests that complex V subunits are mostly found unassembled (Figure S1B). In plants, additional NADH dehydrogenases and ubiquinol oxidases offer alternatives routes for electrons in the respiratory chain, by-passing complex I and complexes III/IV, respectively. These so-called alternative pathways were found to be more abundant in *Viscum* than in *Arabidopsis* (Figure 3B).

The altered OXPHOS system, in particular the dramatic decrease in the protein levels of ATP synthase, suggests that ATP production may not be the primary function of mitochondria in *Viscum*. Using ^{14}C-glucose isotopes, we estimated respiratory fluxes in leaf discs of *Viscum* and *Arabidopsis*. CO_2 can be released from the C1 position by the action of non-mitochondrial catabolic reactions (pentose phosphate pathway) whereas CO_2 evolution from the C3 and C4 positions represents mitochondrial reactions (pyruvate decarboxylase, malic enzyme). We did not observe a major difference in the rate of CO_2 released from ^{14}C3,^{14}C4 glucose in the first 2 hours, but from then on, the rate in *Arabidopsis* leaves was greater than in *Viscum* (Figure 4A). In contrast, the CO_2 release from ^{14}C1 glucose was found to be higher in *Viscum* than in *Arabidopsis* leaf discs at all time points measured (Figure 4B). The ratio of CO_2 evolution from ^{14}C1 glucose to ^{14}C3,^{14}C4 glucose provides a proxy for the relative activity of the TCA cycle with respect to other processes of carbohydrate oxidation. This ratio was constant in *Arabidopsis*, indicating a well coupled respiratory pathway. In *Viscum*, this ratio was increased (Figure 4C), suggesting a redirection of carbon metabolic flux from the TCA cycle to glycolysis.

Taken together, our results show a decrease in several mitochondrial functions in the parasitic plant *Viscum album*. Although our analysis was limited to two tissues, buds and leaves, harvested in the spring, the findings from different methods are consistent and the proteomics data are reproducible using material from two different populations, in the UK and in Germany (Table S1). Consistent with the absence of the *nad* genes from the mitogenome [6,10], complex I could not be detected, neither by in-gel activity staining nor proteomic approaches. Complex I pumps 4 protons across the inner mitochondrial

membrane for every NADH molecule oxidised [19], making it a major contributor to the proton gradient required for ATP synthesis. *Arabidopsis* mutants lacking complex I display increased glycolytic fluxes to produce ATP [16,20]. Similarly, *Viscum* has rearranged its metabolism to generate ATP through glycolysis rather than mitochondrial respiration. The shift in ATP metabolism is reminiscent of the Warburg effect in cancer cells [21] and in Baker's yeast [22], where energy is produced by a high rate of glycolysis accompanied by the redirection of pyruvate towards lactate production, away from the TCA cycle. However, such an energy strategy requires high levels of glycolytic substrates, which in the hemiparasitic *Viscum* can either be supplied by its own photosynthetic capacity, or come from the host. The physiology of *Viscum* is not well characterized, owing to the complexity of the relationship between two rather slow-growing plant species. However, it is thought that the photosynthesis rate of *Viscum* is low [23]. Once the seedling is established, high transpiration rates [24] suggest a significant flux of carbon from the host of up to 80 % of the total carbon [25]. This value would be compatible with the high demand for carbohydrates to sustain energy production from glycolysis.

The mitochondrial reductive evolution seen in *Viscum* is not as severe as that in the plastid genomes (plastomes) of holoparasitic plants, where, as plants become less dependent on their own photosynthetic capability, loss or pseudogenisation of genes in the plastome leads to complete loss of photosynthesis [2,26]. Perhaps the most striking example of this reductive evolution is the giant "carrion flower" from the Philippines, *Rafflesia lagascae*, that may have lost its entire plastome [27]. So far, parasitic plants, including hemiparasites other than mistletoe, have shown little evidence of mitochondrial gene loss and reductive evolution [27-30], possibly indicating that it is specific to the genus *Viscum* or the order Santalales. Interestingly, the widely divergent parasitic species within the Santalales have all retained photosynthesis. Although it is currently not known how many species have lost complex I, it seems possible that diminished mitochondrial capacity precludes loss of photosynthesis, as this would remove an important source of ATP and reducing equivalents. To provide further insight into the evolution and function of plant mitochondria in relation to the adoption of parasitic lifestyles, systematic phylogenomic studies are urgently needed.

Acknowledgements

This work was supported by the John Innes Foundation and the Max Planck Society.

Author contributions

Conceptualization, AEM, RB, JB and EHM; Methodology, AEM, JB and EHM; Investigation, AEM, APH, JL and EHM; Writing, AEM, JB and EHM with revisions from all other authors.

Declaration of Interests

The authors declare no competing interests.

References

1. Jackson, A.P., Otto, T.D., Aslett, M., Armstrong, S.D., Bringaud, F., Schlacht, A., Hartley, C., Sanders, M., Wastling, J.M., Dacks, J.B., *et al.* (2016). Kinetoplastid phylogenomics reveals the evolutionary innovations associated with the origins of parasitism. Curr. Biol. *26*, 161–172.

2. Wicke, S., Müller, K.F., dePamphilis, C.W., Quandt, D., Bellot, S., and Schneeweiss, G.M. (2016). Mechanistic model of evolutionary rate variation en route to a nonphotosynthetic lifestyle in plants. Proc. Natl. Acad. Sci. *113*, 9045–9050.

3. Stairs, C.W., Leger, M.M., and Roger, A.J. (2015). Diversity and origins of anaerobic metabolism in mitochondria and related organelles. Philos. Trans. R. Soc. B Biol. Sci. *370*, 20140326.

4. Karnkowska, A., and Hampl, V. (2016). The curious case of vanishing mitochondria. Microb. Cell *3*, 491–494.

5. Skippington, E., Barkman, T.J., Rice, D.W., and Palmer, J.D. (2015). Miniaturized mitogenome of the parasitic plant *Viscum scurruloideum* is extremely divergent and dynamic and has lost all *nad* genes. Proc. Natl. Acad. Sci. U. S. A. *112*, E3515-24.

6. Petersen, G., Cuenca, A., Møller, I.M., and Seberg, O. (2015). Massive gene loss in mistletoe (*Viscum*, Viscaceae) mitochondria. Sci. Rep. *5*, 17588.

7. Liu, Y., Medina, R., and Goffinet, B. (2014). 350 My of mitochondrial genome stasis in mosses, an early land plant lineage. Mol. Biol. Evol. *31*, 2586–2591.

8. Sloan, D.B., Alverson, A.J., Chuckalovcak, J.P., Wu, M., McCauley, D.E., Palmer, J.D., and Taylor, D.R. (2012). Rapid evolution of enormous, multichromosomal genomes in flowering plant mitochondria with exceptionally high mutation rates. PLoS Biol. *10*.

9. Mower, J.P., Sloan, D.B., and Alverson, A.J. (2012). Plant mitochondrial genome diversity: the genomics revolution. In Plant Genome Diversity Volume 1, J. F. Wendel et al, eds. (Springer-Verlag Wein), pp. 123-144.

10. Skippington, E., Barkman, T.J., Rice, D.W., and Palmer, J.D. (2017). Comparative mitogenomics indicates respiratory competence in parasitic *Viscum* despite loss of complex I and extreme sequence divergence, and reveals horizontal gene transfer

and remarkable variation in genome size. BMC Plant Biol. *17*, 49.

11. Kobayashi, Y., Knoop, V., Fukuzawa, H., Brennicke, A., and Ohyama, K. (1997). Interorganellar gene transfer in bryophytes: The functional *nad7* gene is nuclear encoded in Marchantia polymorpha. Mol. Gen. Genet. *256*, 589–592.

12. Gabaldón, T., Rainey, D., and Huynen, M.A. (2005). Tracing the evolution of a large protein complex in the eukaryotes , nadh : ubiquinone oxidoreductase (complex i). J. Mol. Biol. *348*, 857–870.

13. James, T.Y., Pelin, A., Bonen, L., Ahrendt, S., Sain, D., Corradi, N., and Stajich, J.E. (2013). Shared signatures of parasitism and phylogenomics unite cryptomycota and microsporidia. Curr. Biol. *23*, 1548–1553.

14. Flegonotov, P., Michalek, J., Janouskovec, J., Lai, D.H., Jirku, M., Hajduskova, E., Tomcala, A., Otto, T.D., Keeling, P.J., Pain, A., *et al.* (2015). Divergent mitochondrial respiratory chains in phototrophic relatives of apicomplexan parasites. Mol Biol Evol *32*, 1115–1131.

15. Sweetlove, L.J., Taylor, N.L., and Leaver, C.J. (2007). Isolation of intact, functional mitochondria from the model plant *Arabidopsis thaliana*. Methods Mol. Biol. *372*, 125–136.

16. Kühn, K., Obata, T., Feher, K., Bock, R., Fernie, A.R., and Meyer, E.H. (2015). Complete mitochondrial complex I deficiency induces an up-regulation of respiratory fluxes that is abolished by traces of functional complex i. Plant Physiol. *168*, 1537–1549.

17. Meyer, E.H., Tomaz, T., Carroll, A.J., Estavillo, G., Delannoy, E., Tanz, S.K., Small, I.D., Pogson, B.J., and Millar, a H. (2009). Remodeled respiration in *ndufs4* with low phosphorylation efficiency suppresses *Arabidopsis* germination and growth and alters control of metabolism at night. Plant Physiol. *151*, 603–619.

18. Zonneveld, B.J.M. (2010). New record holders for maximum genome size in eudicots and monocots. J. Bot. *2010*, Article ID 527357.

19. Jones, A.J.Y., Blaza, J.N., Varghese, F., and Hirst, J. (2017). Respiratory complex I in *Bos taurus* and paracoccus denitrificans pumps four protons across the membrane for every NADH oxidized. J. Biol. Chem. *292*, 4987–4995.

20. Fromm, S., Senkler, J., Eubel, H., Peterhänsel, C., and Braun, H.P. (2016). Life

without complex I: proteome analyses of an *Arabidopsis* mutant lacking the mitochondrial NADH dehydrogenase complex. J. Exp. Bot. *67*, 3079-93.

21. Liberti, M. V, and Locasale, J.W. (2017). The warburg effect : how does it benefit cancer cells? Trends Biochem. Sci. *41*, 211–218.

22. Diaz-Ruiz, R., Rigoulet, M., and Devin, A. (2011). The Warburg and Crabtree effects: On the origin of cancer cell energy metabolism and of yeast glucose repression. Biochim. Biophys. Acta - Bioenerg. *1807*, 568–576.

23. Strong, G., Bannister, P., and Burritt, D. (2000). Are mistletoes shade plants? co2 assimilation and chlorophyll fluorescence of temperate mistletoes and their hosts. Ann. Bot. *85*, 511–519.

24. Escher, P., Peuke, A.D., Bannister, P., Fink, S., Hartung, W., Jiang, F., and Rennenberg, H. (2008). Transpiration, CO2 assimilation, WUE, and stomatal aperture in leaves of *Viscum album* (L.): Effect of abscisic acid (ABA) in the xylem sap of its host (*Populus x euamericana*). Plant Physiol. Biochem. *46*, 64–70.

25. Těšitel, J., Plavcová, L., and Cameron, D.D. (2010). Interactions between hemiparasitic plants and their hosts: The importance of organic carbon transfer. Plant Signal Behav. *5*, 1072–1076.

26. Wicke, S., Müller, K.F., de Pamphilis, C.W., Quandt, D., Wickett, N.J., Zhang, Y., Renner, S.S., and Schneeweiss, G.M. (2013). Mechanisms of functional and physical genome reduction in photosynthetic and nonphotosynthetic parasitic plants of the broomrape family. Plant Cell *25*, 3711–25.

27. Molina, J., Hazzouri, K.M., Nickrent, D., Geisler, M., Meyer, R.S., Pentony, M.M., Flowers, J.M., Pelser, P., Barcelona, J., Inovejas, S.A., *et al.* (2014). Possible loss of the chloroplast genome in the parasitic flowering plant *Rafflesia lagascae* (Rafflesiaceae). Mol. Biol. Evol. *31*, 793–803.

28. Xi, Z., Wang, Y., Bradley, R.K., Sugumaran, M., Marx, C.J., Rest, J.S., and Davis, C.C. (2013). Massive mitochondrial gene transfer in a parasitic flowering plant clade. PLoS Genet. *9*, 1–10.

29. Bellot, S., Cusimano, N., Luo, S., Sun, G., Zarre, S., Gröger, A., Temsch, E., and Renner, S.S. (2016). Assembled plastid and mitochondrial genomes, as well as nuclear genes, place the parasite family cynomoriaceae in the saxifragales. Genome Biol. Evol. *8*, 2214–2230.

30. Fan, W., Zhu, A., Kozaczek, M., Shah, N., Pabón-Mora, N., González, F., and Mower, J.P. (2016). Limited mitogenomic degradation in response to a parasitic lifestyle in Orobanchaceae. Sci. Rep. *6*, 36285.

31. Balk, J., and Leaver, C.J. (2001). The PET1-CMS mitochondrial mutation in sunflower is associated with premature programmed cell death and cytochrome c release. Plant Cell *13*, 1803–1818.

32. Meyer, E.H., Solheim, C., Tanz, S.K., Bonnard, G., and Millar, A. H. (2011). Insights into the composition and assembly of the membrane arm of plant complex I through analysis of subcomplexes in Arabidopsis mutant lines. J. Biol. Chem. *286*, 26081–26092.

33. Sabar, M., Balk, J., and Leaver, C.J. (2005). Histochemical staining and quantification of plant mitochondrial respiratory chain complexes using blue-native polyacrylamide gel electrophoresis. Plant J *44*, 893–901.

34. Sun, F., Wang, X., Bonnard, G., Shen, Y., Xiu, Z., Li, X., Gao, D., Zhang, Z., and Tan, B.C. (2015). Empty pericarp7 encodes a mitochondrial E-subgroup pentatricopeptide repeat protein that is required for ccmFN editing, mitochondrial function and seed development in maize. Plant J. *84*, 283–295.

35. Feissner, R., Xiang, Y., and Kranz, R.G. (2003). Chemiluminescent-based methods to detect subpicomole levels of c-type cytochromes. Anal. Biochem. *315*, 90–94.

36. Cox, J., and Mann, M. (2008). MaxQuant enables high peptide identification rates, individualized p.p.b.-range mass accuracies and proteome-wide protein quantification. Nat. Biotechnol. *26*, 1367–1372.

37. Rees, T. A, and Beevers, H. (1960). Pathways of Glucose Dissimilation in Carrot Slices. Plant Physiol. *35*, 830–8.

38. Nunes-Nesi, A., Carrari, F., Lytovchenko, A., Smith, A.M.O., Loureiro, M.E., Ratcliffe, R.G., Sweetlove, L.J., and Fernie, A.R. (2005). Enhanced photosynthetic performance and growth as a consequence of decreasing mitochondrial malate dehydrogenase activity in transgenic tomato plants. Plant Physiol. *137*, 611–22.

Figure Legends

Figure 1. Ultrastructure and purification of *Viscum album* mitochondria

Electron microscopy images of mitochondria from *Viscum album* leaves. Scale bar (left and middle) = 500 nm. White box indicates area shown in right panel, where scale bar = 100 nm. (B) *Viscum album* branch with two leaves and terminal bud (arrow). The buds were harvested to purify mitochondria. Scale bar = 1 cm. (C) Membranes from buds were separated by centrifugation on a continuous gradient of Percoll, PVP-40 and sucrose, with a 40% (w/v) Percoll cushion in the bottom. The mitochondria fraction (Mit) is marked by an arrow. (D) Immuno-blot analysis of two mitochondrial proteins, showing enrichment in the mitochondrial fraction compared to total extract. VDAC, voltage-dependent anion channel of the outer mitochondrial membrane protein; PDH E1α, subunit of the pyruvate dehydrogenase (PDH) complex in the mitochondrial matrix. Equal amounts of protein were loaded in each lane, as confirmed by Ponceau staining.

Figure 2. Activity of respiratory complexes in *Viscum album.*

(A-E) BN-PAGE analysis of mitochondrial samples from *Arabidopsis thaliana* tissue culture and *Viscum album* buds (A) Protein complexes visualised with Coomassie staining. (B) NADH dehydrogenase activities were visualised with NADH:NBT staining, revealing complex I in *Arabidopsis* but not *Viscum*, and LPD2, lipoamide dehydrogenase 2, in both samples. (C) Complex II activity was visualised with succinate:NBT staining. (D) Heme-dependent peroxidase activity of complex III was visualised using chemiluminescence. (E) Complex IV activity was visualised with Cytc:DAB staining, using a preparation of *Viscum album* mitochondria that contained some chloroplast proteins. The colour balance of the gels was adjusted to enhance the enzyme stains relative to the background.

Figure 3. Composition of *Viscum album* mitochondria.

Proteome analysis of *Viscum* mitochondria (see also Figure S1 and Data S1). (A) Table presenting a subset of the GO enrichment analysis performed on the list of identified proteins, only significantly enriched (p value < 0.05) processes are shown. The full dataset is available as Table S2. The fold enrichment is calculated by dividing the *identified* number of proteins of a biological process by the *expected* number of proteins to be identified if every

protein had the same probability to be identified. Note that this analysis is not quantitative and the *Arabidopsis* proteome was used for the *Viscum* analysis. (B) Quantification of mitochondrial proteins identified in complex mixture analysis and BN-PAGE. Label-free quantification data were obtained for both proteomic approaches and combined to obtain an overview of the relative abundance of proteins involved in a given pathway in *Viscum* mitochondria (Data S2). Top panel, scheme summarising the main mitochondrial functions. The arrows indicate the relative abundance of proteins from each pathway in *Viscum* compared to the same proteins in *Arabidopsis*. Green: increased (more than 110% of *Arabidopsis*), Yellow: similar (between 90% and 110% of *Arabidopsis*), Orange: slightly decreased (between 75% and 90% of *Arabidopsis*), Red: decreased (less than 75% of *Arabidopsis*). Bottom panel, representation of the respiratory chain, complexes are shown as orange boxes, the alternative pathways as green circles, electron transfer as grey arrows and proton transfer as black arrows. As no complex I subunits were identified, complex I is shown as a white box. The proteins identified are indicated below the complex they belong to. The relative amount of each complex was calculated by obtaining the mean value of the different identified subunits (Data S2). Proteins indicated in grey were not used for quantification as no common peptide between *Arabidopsis* and *Viscum* was identified.

Figure 4. Metabolic flux through glycolysis is higher than TCA cycle in *Viscum*

Metabolic flux analysis of leaf disks from *Arabidopsis thaliana* and *Viscum album*. Glucose labelled with radioactive carbon (^{14}C) at position 1 (C1) or position 3 and 4 (C3, C4), were fed to illuminated leaf disks and the resulting $^{14}CO_2$ measured every hour. $^{14}CO_2$ from addition of C1-labelled glucose corresponds to metabolic flux through the pentose phosphate pathway which is used as a proxy for glycolysis (A) and from C3, C4 corresponds to metabolic flux through pyruvate decarboxylase and malic enzyme which is used as a proxy for the TCA cycle (B). Each point represents the mean ± SE (n=4). The ratio between the two (C1/C3,C4) can be calculated and used to infer relative rates (C). dpm, disintegrations per minute, gFW, grams fresh weight.

STAR Methods

CONTACT FOR REAGENT AND RESOURCE SHARING

Further information and requests for resources and reagents should be directed to and will be fulfilled by the Lead Contact, Etienne Meyer (emeyer@mpimp-golm.mpg.de)

EXPERIMENTAL MODEL AND SUBJECT DETAIL

Viscum album plants were harvested from locations in the UK and Germany between March and July, from various host species (*Acer campestre*; *Acer saccharum*; *Malus pumila*; *Salix alba, Sorbus aucuparia, Prunus cerasifera*). Detailed information on the source material is given in Table S1. Leaf buds were harvested for use in biochemical and proteomic assays. Leaf material was used for electron microscopy and flux analysis.

Arabidopsis thaliana plants (ecotype Columbia-0) were grown under long day conditions (16h light 120 $\mu E.m^{-2}.s^{-1}$, 22°C, 8h dark at 20°C). Callus lines were generated from root tissue and grown on agar plates containing Gamborg B5 medium, 2% (w/v) glucose, 0.5 mgL^{-1} 2,4-dichlorophenoxyacetic acid and 0.05 mgL^{-1} kinetin.

METHOD DETAILS

Electron Microscopy

For ultrastructural analysis leaf samples were fixed in 2.5% glutaraldehyde in 50 mM sodium cacodylate (pH 7.4) containing 5 mM $CaCl_2$ for 1 hour under vacuum. Fixation was continued at 4°C overnight. Post-fixation with 1% OsO_4 and 0.8% $K_3Fe(CN)_6$ in 50 mM cacodylate buffer (pH 7.4) was carried out for 2 hours at 4°C. After rinsing the leaf samples in cacodylate buffer, dehydration and embedding in Epon812 (Science Services) were carried out following standard protocols. Ultrathin sections (50-70 nm) were cut with diamond knives. For electron microscopy, thin sections were stained with 2% uranyl acetate and lead citrate and examined in a Zeiss EM 912 Omega transmission electron microscope (Carl Zeiss).

Mitochondrial purification

Mitochondria were purified from *Viscum album* leaf buds, *Arabidopsis thaliana* rosette leaves and cell culture. The material was ground at 4°C in extraction buffer (0.3 M sucrose, 5 mM tetrasodium pyrophosphate, 10 mM KH2PO4, pH 7.5, 2 mM EDTA, 1% [w/v] polyvinylpyrrolidone40, 1% [w/v] bovine serum albumin, 5 mM Cys, and 20 mM ascorbic acid) using mortar and pestle. After filtration through two layers of Miracloth (Millipore), the retained material was ground and filtered another time. The filtrates were pooled and centrifuged for 5 min at 2,000 x *g*, and the supernatant was centrifuged for 10 min at 20,000 x *g*. The pellet was resuspended in wash buffer (0.3 M sucrose, 1 mM EGTA, and 10 mM MOPS-KOH, pH 7.2) and subjected to the same low-speed (2,000 x *g*) and high-speed (20,000 x *g*) centrifugations. For *Viscum* a sample was taken after differential centrifugation and used for complex IV detection. Further purification was performed on *Viscum* and *Arabidopsis* rosette leaf samples using a 0 - 4.4% (v/v) polyvinylpyyrolidine-40 gradient in 28% (v/v) Percoll, with a 40% Percoll cushion at the base to separate mitochondrial and thylakoid fractions. The gradient was centrifuged at 40,000 x *g* for 45 min. The white band located at the bottom of the gradient (see figure 1C?) was collected and washed three times in wash buffer. Protein concentration was determined using the Bradford method (Bio-Rad Protein Assay).

Protein blot analysis

Total leaf bud cell extract or purified mitochondria from *Viscum album* were mixed with Laemmli buffer (2% [w/v] SDS, 125 mM Tris-HCl, 10% [w/v] glycerol, 0.04% [v/v] β-mercaptoethanol, and 0.002% [w/v] bromophenol blue, pH 6.8) and separated on a 15% SDS-PAGE gel. Proteins were transferred under semi-dry conditions to nitrocellulose membrane (Protran™). Equal loading and transfer was confirmed using Ponceau S stain. Proteins were labelled with antibodies and detected using secondary horseradish peroxidase-conjugated antibodies and chemiluminescence (0.1 M Tris-HCl, pH 8.0, 0.11 mg ml^{-1} 3-aminophthalhydrazide (luminol), 16 µg ml^{-1} p-coumaric acid and 0.009% H_2O_2. Mouse monoclonal antibodies against the E1α subunit of pyruvate dehydrogenase and VDAC (GTMA) are as previously reported [31], and both were used at a dilution of 1 in 1000.

Blue-Native PAGE and activity staining

Mitochondrial samples were subjected to Blue-Native-PAGE as described previously [32,16]. Mitochondrial proteins were solubilized with dodecylmaltoside (1% [w/v] final) in ACA buffer (750 mM amino caproic acid, 0.5 mM EDTA, and 50 mM Tris-HCl, pH 7.0) and incubated 20 min at 4°C. The samples were centrifuged for 10 min at 20,000 x *g*, and Serva Blue G (0.25% [v/v] final) was added to the supernatant. The samples were loaded onto a 4.5% to 16% polyacrylamide gradient gel prepared in 0.25 M amino caproic acid, 25 mM Bis-Tris-HCl pH 7. The migration was performed for 45 min at 100 V followed by 14 h at 400 V in cathode buffer (50 mM tricine, 12.5 mM Bis-Tris-HCl pH 7, 0.02% Coomassie G250) and anode buffer (50 mM Bis-Tris-HCl pH 7).

Activity stains were carried out as described previously [33]. Briefly, gels were equilibrated in buffer without staining reagents for 10 min. For complex I, NADH dehydrogenase activity was visualized with 0.1 M Tris-HCl, pH 7.4, 0.2 mM NADH and 0.1 % (w/v) nitro-blue tetrazolium (NBT); For complex II, electron transfer from succinate was shown using 50 mM KH_2PO_4, pH 7.4, 0.1 mM ATP, 10 mM succinate, 0.2 mM phenazine methosulfate, 0.2 % (w/v) NBT; For complex IV, oxidation activity was visualized using 50 mM KH_2PO_4, pH 7.4, 1 mg ml^{-1} cytochrome *c*, 0.1 % (w/v) 3,3'-diaminobenzidine. After the desired staining intensity was reached, the reaction was stopped using a solution of 45% (v/v) methanol and 5% (v/v) acetic acid, followed by washes in the same solution to remove excess Coomassie Blue dye. For detection of complex III proteins were transferred to PVDF membrane and detected by chemiluminescence [34,35].

Mass spectrometry

For the analysis of whole mitochondria, 10 µg of mitochondrial protein were solubilized in 6 M urea, 2 M thiourea, reduced with 5 mM DTT and alkylated with 15 mM iodoacetamide. After dilution to 1.5 M urea with 10 mM Tris-HCL pH 8.0, trypsin digestion was performed for 16 h. Lanes of 1D BN-PAGE were cut into 18 slices. Gel slices were prepared for mass spectrometry by trypic in-gel digestion as described previously [32]. Gel slices were washed three times with 50% acetonitrile, 50 mM NH_4HCO_3, reduced with 10 mM DTT and alkylated with 55 mM iodoacetamide, 50 mM NH_4HCO_3 for 30 min prior to digestion with 10 µg ml^{-1} trypsin for 16 h. Peptides from both preparations were purified using Ziptips (Millipore) according to the manufacturer instructions. The peptides were resuspended in 5% (v/v) acetonitrile, 0,1 % (v/v) formic acid, and analyzed by LC-MS/MS. Peptides were separated on a C18 reverse phase analytical column (Acclaim PepMap100, Thermo Fisher Scientific) using an Easy-nLC 1000 liquid chromatograph system (Thermo Fisher Scientific). Peptides were eluted using a non-linear 5% - 34% (v/v) acetonitrile gradient in 0.1% (v/v) formic acid

and 5% (v/v) DMSO at a flow of 300 nl.min^{-1}. The gradient lasted 28 min for peptides obtained after in-gel digestion and 72 min for peptides obtained after the digestion of whole mitochondria. After the gradient, the column was cleaned for 10 min with 85% (v/v) acetonitrile in 0.1% (v/v) formic acid and 5% (v/v) DMSO. Eluted peptides were transferred to an NanoSpray Ionization source and sprayed into an Orbitrap Q-Exactive Plus mass spectrometer (Thermo Fisher Scientific). The MS was run in positive ion mode. For full MS scans, the following settings were used, resolution: 70000, AGC target: 3E6, maximum injection time: 100 ms, scan range: 200 to 2000 m/z. For dd-MS^2, the following settings were used, resolution: 175000, AGC target: 1E5, maximum injection time: 50 ms, loop count: 15, isolation window: 4.0 m/z, NCE: 30. The following Data-dependent settings were used: underfill ratio: 1%; apex trigger: off; charge exclusion: unassigned, 1, 5, 5–8, >8; peptide match: preferred; exclude isotypes: on; dynamic exclusion: 20.0 sec.

To qualitatively assess the mass spectrometry runs of the whole mitochondria samples, we used MASCOT (Matrix Science). The raw files obtained from Xcalibur were converted into mgf files using MSConvert (Proteowizard). We then performed database searched using an in-house database containing Arabidopsis proteins (TAIR10) and translated sequences of *Viscum album* mitochondrial genes [10]. The search parameters used are the following: missed cleavage: 1, fixed modification: carbamidomethyl (C), variable modification: Oxidation (M), peptide tolerance: 10 ppm, MS/MS tolerance: 0.6 Da, peptide charge: 2+/3+ and 4+, decoy activated. During the search, every time a protein sequence from the database is tested, a random (decoy) sequence of the same length is automatically generated and tested. The numbers obtained are presented in Data S1.

Flux analysis

Estimation of respiratory fluxes by following $^{14}CO_2$ evolution was carried out as described previously [37,38]. Leaf discs (7 mm in diameter) were incubated in 50 mM MES-KOH, pH 6.5 containing 0.3 mM of glucose labelled with 6.2 MBq.mmol^{-1} of ^{14}C at position 1 or positions 3 and 4 (ARC0120A and ARC0211, respectively, American Radiolabelled Chemicals) in closed flasks. Evolved $^{14}CO_2$ was trapped with 10% (w/v) KOH and the trap was replaced every hour. The KOH solution was mixed with scintillation cocktail (Rotizint Eco Plus, Roth) and radioactivity was determined by a liquid scintillation counter (LS6500, Beckman Coulter).

QUANTIFICATION AND STATISTICAL ANALYSIS

Quantification of the mitochondrial proteins in the proteomic datasets

The raw files obtained from Xcalibur (Thermo Fisher Scientific) were uploaded into MaxQuant (version 1.5.2.8) [36] and queried against an in-house database containing Arabidopsis proteins (TAIR10) and translated sequences of *Viscum album* mitochondrial genes [10]. Default parameters were used, except that label-free quantification (LFQ) and intensity-based absolute quantification (IBAQ) were activated. Intensities values from the evidence table were extracted for each peptide identified in the *Arabidopsis* and *Viscum* samples. An average value was calculated for each protein for which more than one peptide was identified (Data S2).

Legend for Supplemental Excel tables

Data S1

List of proteins identified in the mitochondria fractions isolated from Viscum album using complex mixture LC-MS/MS analysis. Related to Figure 3.

Data S2

Quantification of proteins in two proteomic approaches. Related to Figure 3B.

KEY RESOURCES TABLE

REAGENT or RESOURCE	SOURCE	IDENTIFIER
Antibodies		
Mouse monoclonal anti-PDH E1a	GT Monoclonal Antibodies	PM030
Mouse monoclonal anti-VDAC	GT Monoclonal Antibodies	PM035
Bacterial and Virus Strains		
Biological Samples		
Chemicals, Peptides, and Recombinant Proteins		
Cytochrome *c* from equine heart	Sigma	30396
3,3'-diaminobenzidine tetrahydrochloride hydrate	Sigma	D5637
Nitro-blue tetrazolium	Sigma	N6876
Phenazine methosulfate	Sigma	P9625
Percoll	GE Healthcare	17524.02
Polyvinylpyrrolidone-40	Sigma	PVP40
3-aminophthalhydrazide	ACROS Organics	AC153850050
p-coumaric acid	ACROS Organics	AC121090250
Coomasie Blue G250	Serva	
Trypsin	Sigma	T6567
Glucose, D[1-^{14}C]	American Radiolabelled Chemicals	ARC0120A
Glucose, D-[3,4-^{14}C]	American Radiolabelled Chemicals	ARC0211
Deposited Data		
Experimental Models: Cell Lines		

Experimental Models: Organisms/Strains		
Arabidopsis thaliana (ecotype: Columbia-0)		N/A
Viscum album	refer to Table S1	N/A
Oligonucleotides		
Recombinant DNA		
Software and Algorithms		
Mascot	Matrix science	http://www.matrixscience.com/
Maxquant	[36]	http://www.coxdocs.org/doku.php?id=maxquant:start
MSConvert	Proteowizard	http://proteowizard.sourceforge.net/
Other		

Figure 1

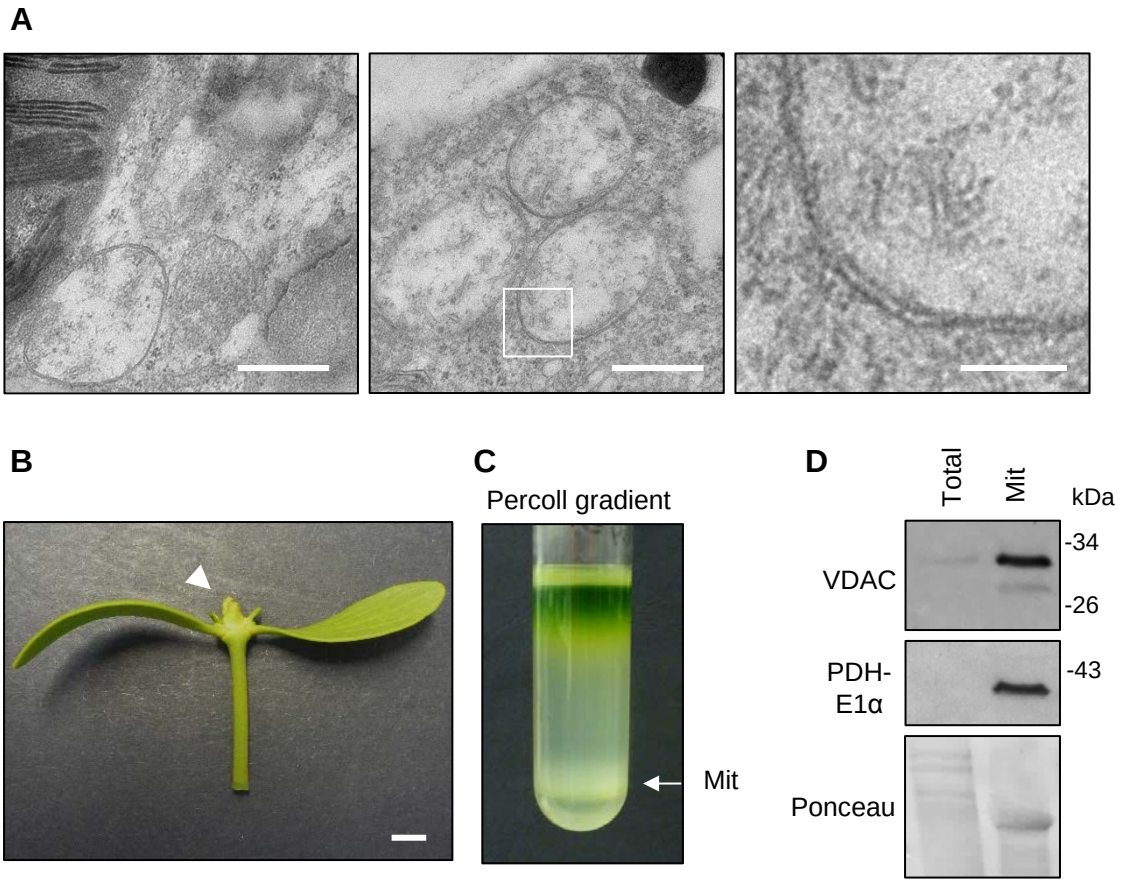
A
B
C
Percoll gradient
Mit
D
Total
Mit
kDa
VDAC
-34
-26
PDH-
E1α
-43
Ponceau

Figure 2

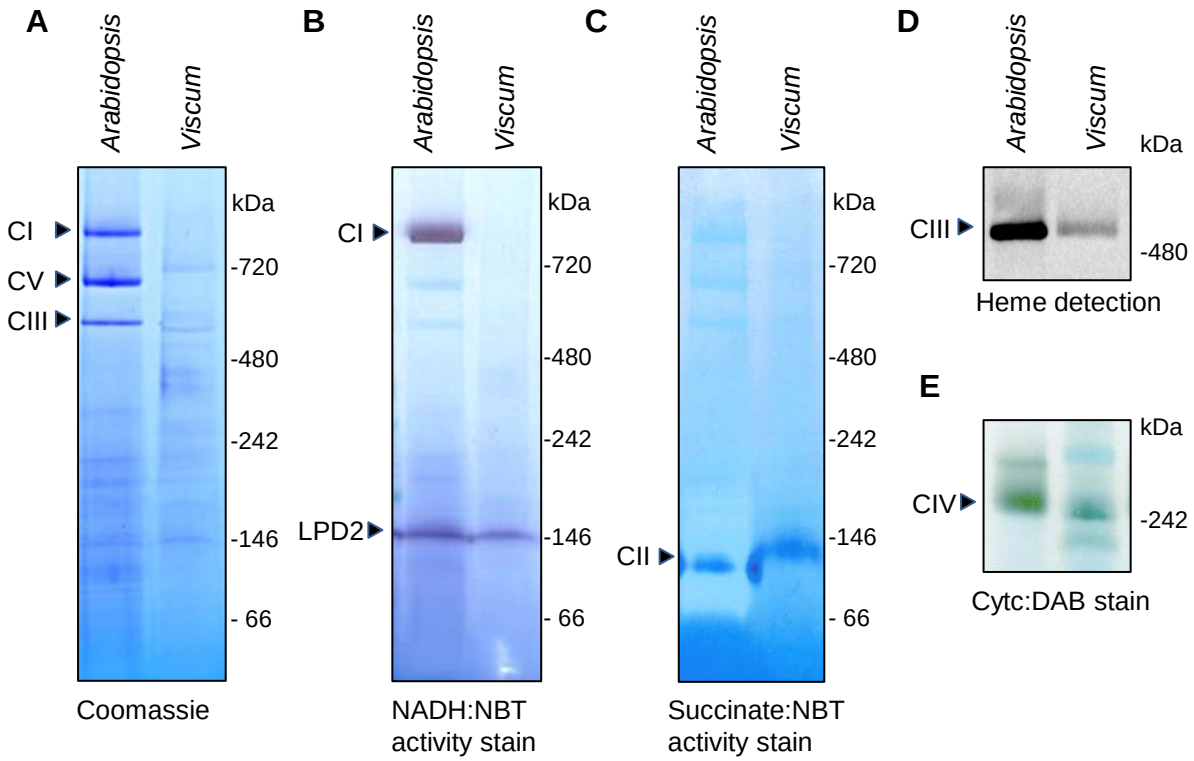
A
Arabidopsis
Viscum
kDa
CI
CV
CIII
-720
-480
-242
-146
- 66
Coomassie
B
Arabidopsis
Viscum
kDa
CI
LPD2
-720
-480
-242
-146
- 66
NADH:NBT
activity stain
C
Arabidopsis
Viscum
kDa
CII
-720
-480
-242
-146
- 66
Succinate:NBT
activity stain
D
Arabidopsis
Viscum
kDa
CIII
-480
Heme detection
E
kDa
CIV
-242
Cytc:DAB stain

Figure 3

A

GO biological process	*Arabidopsis* Fold Enrichment	*Viscum* Fold Enrichment
cellular respiration	12.68	16.81
glycolytic process	6.52	14.61
tricarboxylic acid cycle	13.15	27.5
respiratory electron transport chain	14.94	
mitochondrial ATP synthesis	12.35	
mitochondrion organization	8.87	8.62
mitochondrial transport	9.98	10.58
organic acid metabolic process	4.48	6.46
organic acid catabolic process	9.24	15.81
transmembrane transport	3.05	3.29
cofactor biosynthetic process	4.62	5.9
alpha-amino acid metabolic process	5.07	6.55
nucleotide metabolic process	6.44	7
photorespiration	18.28	13.84
translation	8.91	4.53
response to bacterium	2.68	4.09
response to oxidative stress	2.79	
response to abiotic stimulus	2.55	3
unclassified	0.47	0.56
transcription, DNA-templated	0.25	0.2
regulation of gene expression	0.38	0.31

B

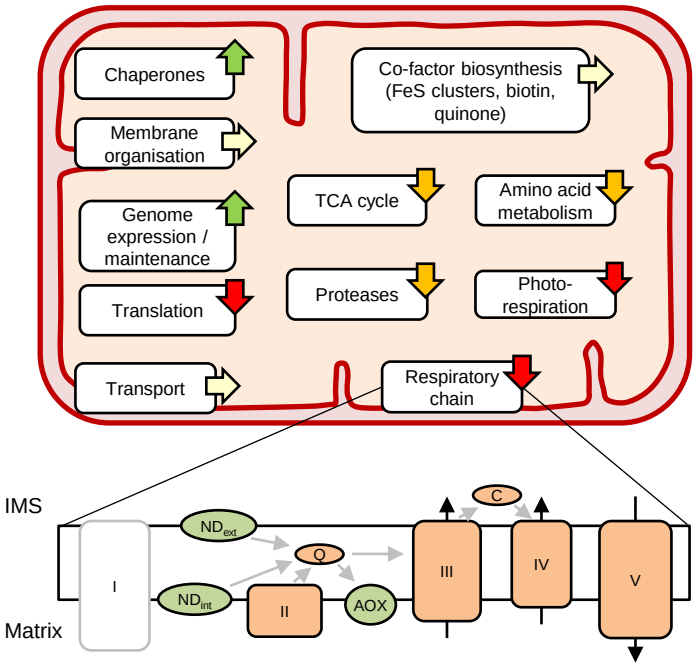

Subunits identified in *Viscum*	NDA1 NDB2	SDH1 SDH2	AOX1A AOX2	CYTc$_1$ Cob MPPβ UCR1 QCR7	Cox1 Cox2 Cox3 COX6b	Atp1 Atp4 Atp6 Atp8	ATPβ ATPδ ATPγ
Relative amount compared to *Arabidopsis*	300%	44%	131%	25%	19%	14%	

Figure 4

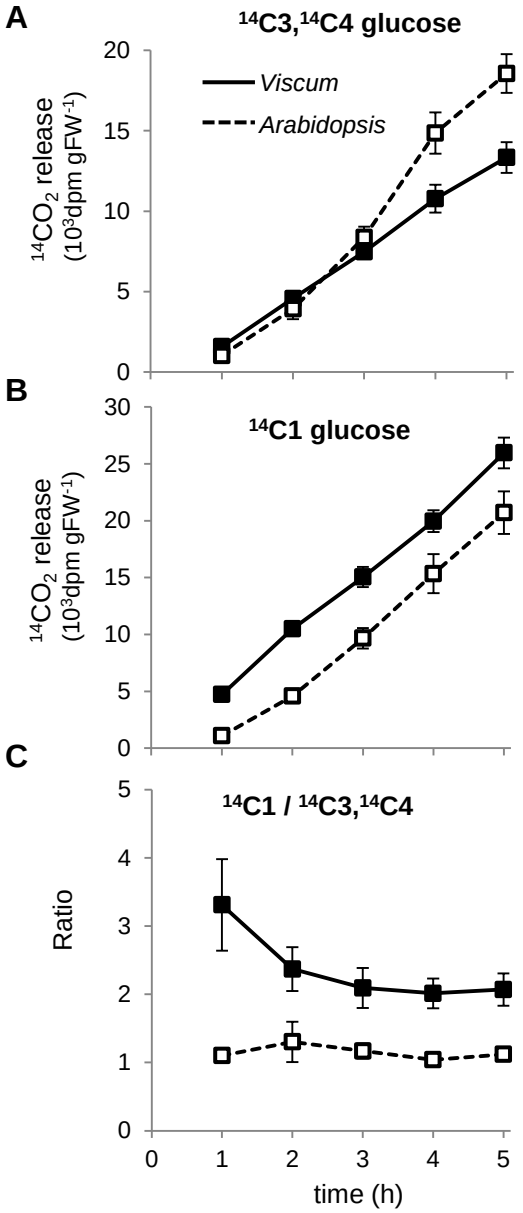
A
^{14}C3,^{14}C4 glucose
Viscum
Arabidopsis
$^{14}CO_2$ release (10^3dpm gFW^{-1})
20
15
10
5
0
B
^{14}C1 glucose
$^{14}CO_2$ release (10^3dpm gFW^{-1})
30
25
20
15
10
5
0
C
^{14}C1 / ^{14}C3,^{14}C4
Ratio
5
4
3
2
1
0
0
1
2
3
4
5
time (h)

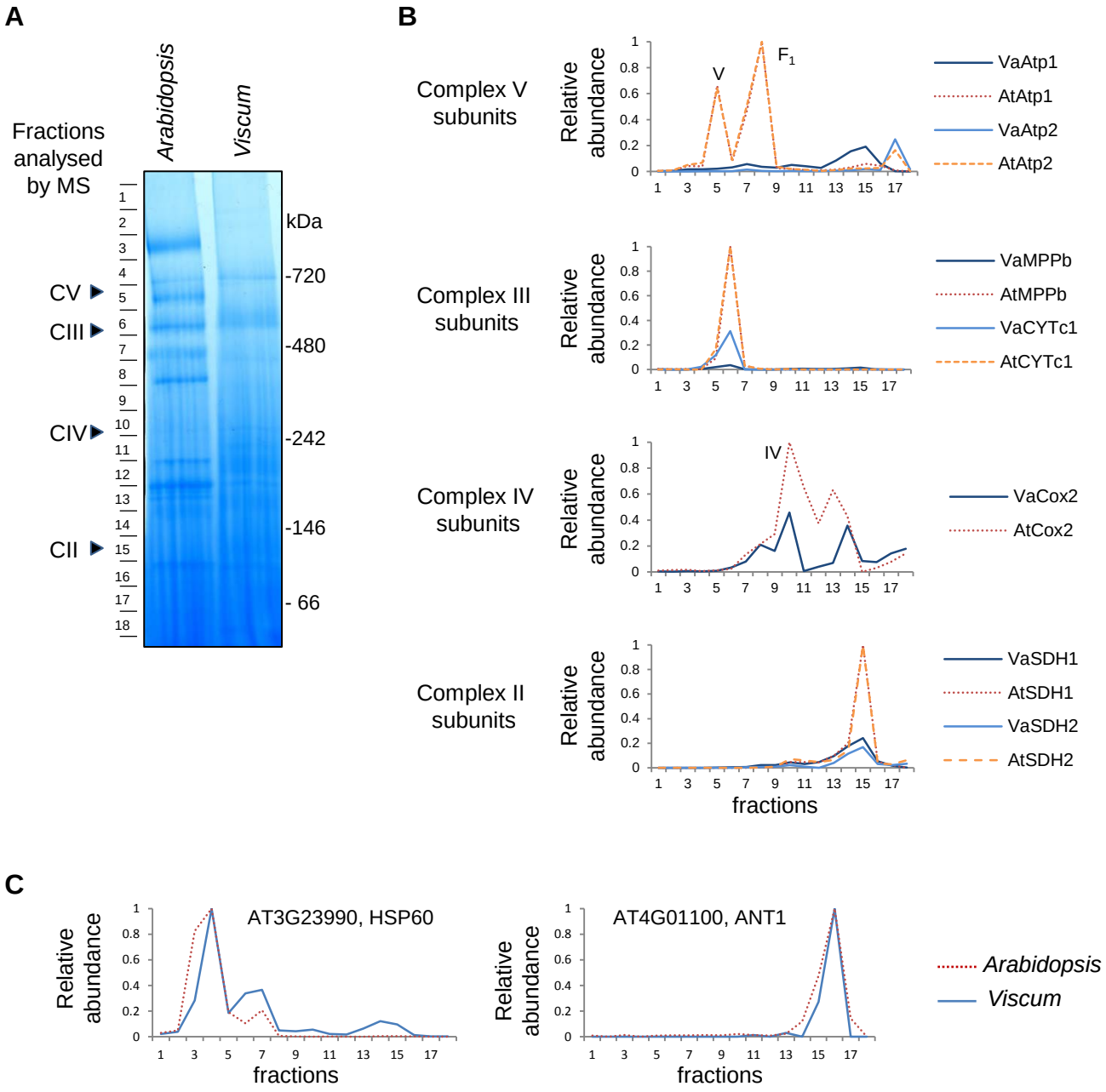

Figure S1. Analysis of respiratory complexes using complexome profiling. Related to Figure 3
(A) Mitochondrial complexes were separated on BN-PAGE and stained using Coomassie blue. Each lane was cut in 18 equal slices, indicated on the left of the gel. The position of complexes II – V is indicated on the left and the molecular weight on the right. (B) Profiles of selected subunits of respiratory complexes. IBAQ values (Intensity-Based Absolute Quantification) were obtained to quantify each subunit in all the fractions. To allow direct comparison between *Arabidopsis* and *Viscum*, the values were normalised for each subunit to the most abundant fraction across both samples. For complex V subunits (top panel), two major peaks are detected in *Arabidopsis*, they correspond to the fully assembled complex V (V) and the F_1 domain of complex V (F_1). Complex IV activity was visualised at 250 kDa (Figure 2E), this size correspond to fraction 10 where the most abundant peak for Cox2 is detected. The peak at ca. 150 kDa (fractions 13-14) has not been characterized previously and might correspond to an assembly intermediate or a disassembly product. Solid blue lines: *Viscum,* Orange dashed lines: *Arabidopsis*. (C) Profile of two housekeeping proteins, HSP60 and ANT.

Table S1
Details of *Viscum album* material used in this study. Related to the STAR Methods section and Figures 1, 2, 3 and 4

Date	Location	Host tree	Tissue	Extraction method	Experiments performed				
					BN-PAGE and activity staining	Complex mixture LC-MS/MS	Proteomic analysis of BN-PAGE	Flux analysis	Electron microscopy
26/03/2017	Cambridge, U.K.	*Acer campestre*	Buds, male	differential centrifugation	X				
17/04/2017	Cambridge, U.K.	*Acer saccharum*	Buds, ?	differential centrifugation	X				
17/04/2017	Cambridge, U.K.	*Malus pumila* “Bramley”	Buds, female	diff. centrifugation and density gradient	X	X			
26/04/2017	Cambridge, U.K.	*Acer campestre*	Buds, male	differential centrifugation	X				
02/05/2017	Potsdam-Golm, Germany	*Salix alba*	Buds, male	diff. centrifugation and density gradient	X	X	X		
25/06/2017	Potsdam-Golm, Germany	*Sorbus aucuparia*	Buds, male	diff. centrifugation and density gradient		X			
19/07/2017	Potsdam-Golm, Germany	*Sorbus aucuparia*	Leaves, male					X	X
10/01/2018	Potsdam-Golm, Germany	*Prunus cerasifera*	Buds, male	diff. centrifugation and density gradient	X				

Table S2

Composition of *Viscum album* mitochondria. Related to Figure 3A

A GO enrichment analysis was performed using the list of *Viscum* mitochondrial proteins obtained after complex mixture LC-MS/MS analysis (Data S1).

reference list: the number of proteins in the reference list that map to the biological process
nb of proteins: indicates how many proteins from the experimental proteome are found in the reference list. The total indicate the size of these proteomes (794 proteins for Arabidopsis, 292 proteins for Viscum)
expected: indicates the number of proteins that should be identified if every of the 27502 proteins in the GO annotation had the same probability to be identified.
Fold enrichment: nb of proteins divided by expected. If >1, it indicates that the biological process is overrepresented in the experimental proteome
P value: p-value as determined by the binomial statistic. This is the probability that the number of genes you observed in this category occurred by chance (randomly), as determined by your reference list.
non significant enrichment (p value > 0.05) are highlighted in red

		Arabidopsis				Viscum			
GO biological process	reference list	nb of proteins (total: 794)	expected	Fold Enrichment	P value	nb of proteins (total: 292)	expected	Fold Enrichment	P value
photosynthesis	233	46	6.74	6.83	3.08E-20	33	2.54	12.98	1.22E-22
fatty acid biosynthetic process	150	16	4.34	3.69	3.06E-02	10	1.64	6.11	1.98E-02
fatty acid oxidation	36	11	1.04	10.57	3.61E-05	10	0.5	25.46	3.72E-08
cellular respiration	120	44	3.47	12.68	6.75E-30	22	1.31	16.81	1.20E-16
glycolytic process	69	13	1.99	6.52	4.77E-04	11	0.75	14.61	1.20E-06
nicotinamide nucleotide metabolic process	113	19	3.27	5.82	4.80E-06	15	1.23	12.17	1.05E-08
tricarboxylic acid cycle	50	19	1.45	13.15	4.83E-12	15	0.55	27.5	9.43E-14
respiratory electron transport chain	44	19	1.27	14.94	5.00E-13	6	0.48	12.5	6.75E-01
mitochondrial ATP synthesis coupled electron transport	28	10	0.81	12.35	3.87E-05	3	0.31	9.82	1.00E+00
proton transport	68	22	1.97	11.19	7.78E-13	4	0.74	5.39	1.00E+00

		Arabidopsis				Viscum			
GO biological process	reference list	nb of proteins (total: 794)	expected	Fold Enrichment	P value	nb of proteins (total: 292)	expected	Fold Enrichment	P value
mitochondrion organization	117	30	3.38	8.87	1.77E-15	11	1.28	8.62	2.52E-04
mitochondrial transport	104	30	3.01	9.98	7.35E-17	12	1.13	10.58	7.08E-06
organic acid metabolic process	1050	136	30.35	4.48	1.11E-44	74	11.45	6.46	1.61E-34
organic acid catabolic process	116	31	3.35	9.24	1.47E-16	20	1.27	15.81	1.97E-14
transmembrane transport	613	54	17.72	3.05	3.66E-09	22	6.69	3.29	3.83E-03
cofactor biosynthetic process	202	27	5.84	4.62	3.20E-07	13	2.2	5.9	1.28E-03
alpha-amino acid metabolic process	280	41	8.09	5.07	2.50E-13	20	3.05	6.55	1.80E-07
nucleotide metabolic process	301	56	8.7	6.44	6.97E-24	23	3.28	7	1.69E-09
photorespiration	53	28	1.53	18.28	1.91E-22	8	0.58	13.84	4.35E-04
translation	567	146	16.39	8.91	4.61E-86	28	6.19	4.53	1.41E-07
response to bacterium	426	33	12.31	2.68	1.50E-03	19	4.65	4.09	8.82E-04
response to oxidative stress	446	36	12.89	2.79	1.76E-04	16	4.87	3.29	1.05E-01
response to abiotic stimulus	1954	144	56.48	2.55	1.93E-21	64	21.31	3	5.95E-12
unclassified	5719	78	165.32	0.47	0.00E+00	35	62.38	0.56	0.00E+00
transcription, DNA-templated	1833	13	52.99	0.25	4.67E-08	4	19.99	0.2	2.75E-02
regulation of gene expression	2652	29	76.66	0.38	2.19E-07	9	28.93	0.31	1.87E-02
regulation of macromolecule metabolic process	2857	26	72.04	0.36	2.35E-07	11	31.17	0.35	3.56E-02

Data S1

Click here to access/download

Supplemental Videos and Spreadsheets

Data S1.xlsx

Click here to access/download

Supplemental Videos and Spreadsheets

Data S2.xlsx